

# High Ionic Conductivity with Low Degradation in A-Site Strontium-Doped Nonstoichiometric Sodium Bismuth Titanate Perovskite

Fan Yang, Huairuo Zhang, Linhao Li, Ian M. Reaney, and Derek C. Sinclair\*

Department of Materials Science and Engineering, University of Sheffield, Sheffield S1 3JD, United Kingdom

## Supporting Information

Oxide-ion conductors are an exciting class of materials.<sup>1</sup> There has been a continued drive for the development of oxide-ion conductors because of their potential applications in various important technological devices such as solid oxide fuel cells (SOFCs), oxygen separation membranes, oxygen sensors, and oxygen pumps.<sup>2–6</sup> In the past decade, the pace of research on oxide-ion conductors has been rapid. A wide range of materials, e.g., ZrO<sub>2</sub> or CeO<sub>2</sub>-based fluorites,<sup>7–10</sup> LaGaO<sub>3</sub>-based perovskites,<sup>11–13</sup> La<sub>2</sub>Mo<sub>2</sub>O<sub>9</sub>-based LAMOX family,<sup>14</sup> lanthanum silicate-based apatites,<sup>15</sup> stabilized  $\delta$ -Bi<sub>2</sub>O<sub>3</sub><sup>16–20</sup> and the Bi<sub>4</sub>V<sub>2</sub>O<sub>11</sub>-based BIMEVOX family<sup>21</sup> have been reported, among which Bi-based materials exhibit the highest known oxygen-ion conductivity.

Despite their attractive levels of oxide-ion conductivity at intermediate temperatures, i.e., 400–600 °C, it is challenging to implement stabilized  $\delta$ -Bi<sub>2</sub>O<sub>3</sub> materials as an electrolyte for intermediate temperature solid oxide fuel cells (ITSOFCs) for two reasons. First, they are prone to chemical reduction/decomposition under the required operating conditions (partial oxygen pressure–temperature,  $p_{\text{O}_2}$ – $T$ ) at the fuel electrode.<sup>22</sup> Second, many stabilized  $\delta$ -Bi<sub>2</sub>O<sub>3</sub> materials are known to suffer from degradation (or aging) of the oxide-ion conductivity in this temperature range due to a combination of phase transformations and anion ordering. The former generally occur at >600 °C, whereas the latter is often dominant at ~500 °C but becomes less pronounced at lower temperatures due to the slower kinetics associated with anion ordering.<sup>18–23</sup> Wachsman and co-workers have demonstrated the first obstacle can be overcome by the creation of bilayer electrolytes, based on Gd-stabilized CeO<sub>2</sub> (GDC) and stabilized  $\delta$ -Bi<sub>2</sub>O<sub>3</sub>.<sup>24,25</sup> In this arrangement, the highly conducting  $\delta$ -Bi<sub>2</sub>O<sub>3</sub> layer is protected from the low  $p_{\text{O}_2}$  at the fuel electrode by the more robust GDC (also an oxide-ion conductor) thus raising the  $p_{\text{O}_2}$  experienced by the  $\delta$ -Bi<sub>2</sub>O<sub>3</sub> sufficiently to avoid chemical reduction/decomposition and therefore taking advantage of its higher oxide-ion conductivity. The same group has studied degradation effects in  $\delta$ -Bi<sub>2</sub>O<sub>3</sub> over many years and has shown that appropriately sized rare earth dopants and codoping with other elements, e.g., Dy and W at various levels can be effective in suppressing the degradation of ionic conductivity at ~500 °C.<sup>18,23,26–28</sup>

In 2014, we reported a new family of oxide-ion conductors based on the ferroelectric perovskite sodium bismuth titanate (Na<sub>0.5</sub>Bi<sub>0.5</sub>TiO<sub>3</sub>, NBT).<sup>29,30</sup> In particular, high levels of oxide-ion conduction were found in bismuth-deficient NBT, i.e., Na<sub>0.50</sub>Bi<sub>0.49</sub>TiO<sub>2.985</sub>, NB<sub>0.49</sub>T. The high ionic conductivity originates from oxygen vacancies generated because of Bi deficiency, as well as high anion mobility as a result of highly

polarizable Bi<sup>3+</sup> with its 6s<sup>2</sup> lone pair electrons and weak Bi–O bonds, which provide pathways with low diffusion barriers.<sup>29,31</sup> The predominant oxide-ion conduction in NB<sub>0.49</sub>T has been confirmed by <sup>18</sup>O diffusion profiles and electromotive force (EMF) measurements, which show an ionic transport number  $t_i > 0.9$  at 600–700 °C.<sup>29</sup> Enhancement of the bulk conductivity ( $\sigma_b$ ) by more than half an order of magnitude was achieved by acceptor-doping Mg<sup>2+</sup> onto the Ti-site (B-site) of NB<sub>0.49</sub>T to create a higher level of oxygen vacancies. Unfortunately, further enhancement of  $\sigma_b$  by increasing the doping level of Mg<sup>2+</sup> has not been achieved. Experimentally, the solubility of Mg<sup>2+</sup> on the Ti-site is rather low, i.e., a Ti-rich secondary phase has been observed in 2 at% Mg-doped NB<sub>0.49</sub>T.<sup>29</sup> Theoretically, first-principles calculations have recently predicted acceptor dopants on the Ti-site to significantly increase the oxygen migration barriers by binding with oxygen vacancies, which suppresses the mobility of oxygen ions and is detrimental to optimizing the ionic conduction.<sup>32</sup> The same study proposed that acceptor doping on the A-site of the perovskite cell may be a more effective method to suppress binding with oxygen vacancies and therefore result in optimization of the ionic conductivity in NBT-based materials.

Here, we report a Sr-doped NB<sub>0.49</sub>T, Na<sub>0.50</sub>Bi<sub>0.47</sub>Sr<sub>0.02</sub>TiO<sub>2.975</sub>, in which Sr<sup>2+</sup> replaces Bi<sup>3+</sup> on the A-site of NBT with the creation of oxygen vacancies. This A-site acceptor doping mechanism enhances  $\sigma_b$  compared with NB<sub>0.49</sub>T perovskite but more importantly, Sr-doped NB<sub>0.49</sub>T exhibits low degradation of  $\sigma_b$  with time at intermediate temperatures, as well as reasonable stability under reducing atmosphere, which makes it a promising electrolyte material for ITSOFCs.

Sr-doped NB<sub>0.49</sub>T ceramics were prepared by the solid-state reaction method. Appropriate amounts of each powder was ball milled and then calcined twice at 800 °C. Pellets were sintered at 1150 °C for 2 h. Sintered pellets were phase-pure by XRD, dense (>95% of the theoretical X-ray density) and with an average grain size of ~5  $\mu\text{m}$  as shown by SEM on thermally etched surfaces. EDX analysis on the polished surface (without thermal etch) shows the composition is close to its nominal value and thus confirms the suggested doping mechanism. Electrical conductivity was obtained from ac impedance spectroscopy. A typical complex impedance plane ( $Z^*$ ) plot of Sr-doped NB<sub>0.49</sub>T showed three arcs, from high to low frequency representing the response from the grains (bulk), grain boundaries and electrode effects, respectively. An

Received: June 23, 2016

Revised: July 26, 2016

Published: July 26, 2016

equivalent circuit of three resistor-constant phase elements (R-CPE) connected in series was used to fit the data. Impedance measurements carried out in N<sub>2</sub>, air, and O<sub>2</sub> showed  $\sigma_b$  to be independent of oxygen partial pressure ( $p_{O_2}$ ), indicating the conduction is predominately ionic in the temperature and  $p_{O_2}$  range studied here. Electromotive force measurement using N<sub>2</sub>/air shows an ionic transport number  $\sim 0.95$  at 600–700 °C, confirming the oxide-ion conduction mechanism in Sr-doped NB<sub>0.49</sub>T. The experimental details and characterization via XRD, SEM, EDX, impedance spectroscopy and equivalent circuit fitting, atmosphere test results and ionic transport numbers are given as Figures S1–S4 and Tables S1 and S2.

Comparison of  $\sigma_b$  for Sr-doped NB<sub>0.49</sub>T with some of the best known oxide-ion conductors is shown in Figure 1. Similar

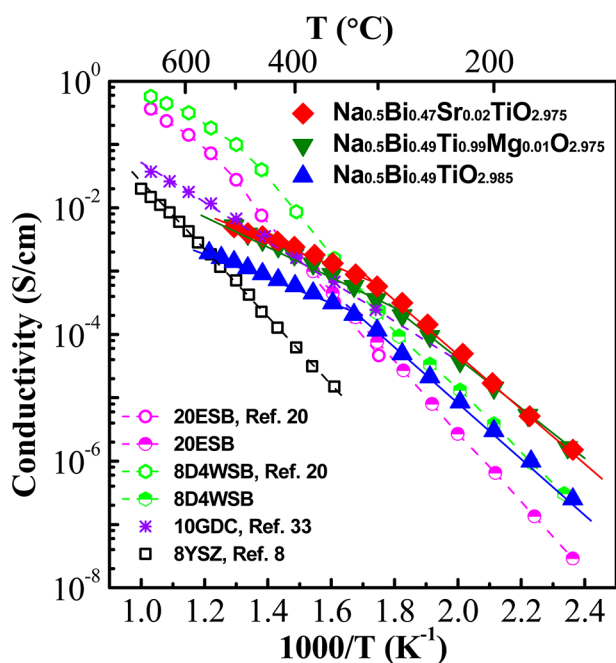
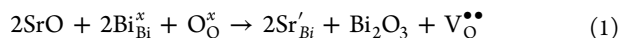


**Figure 1.** Bulk conductivity of Sr-doped, Mg-doped, and undoped NB<sub>0.49</sub>T in comparison with other oxide-ion conductors: (BiO<sub>1.5</sub>)<sub>0.8</sub>(ErO<sub>1.5</sub>)<sub>0.2</sub>, 20ESB;<sup>20</sup> (BiO<sub>1.5</sub>)<sub>0.88</sub>(DyO<sub>1.5</sub>)<sub>0.08</sub>(WO<sub>3</sub>)<sub>0.04</sub>, 8D4WSB;<sup>20</sup> Ce<sub>0.9</sub>Gd<sub>0.1</sub>O<sub>1.95</sub>, 10GDC;<sup>33</sup> Zr<sub>0.852</sub>Y<sub>0.148</sub>O<sub>1.926</sub>, 8YSZ.<sup>8</sup>

to B-site Mg-doping, A-site Sr-doping enhances  $\sigma_b$  by more than half an order of magnitude compared to undoped NB<sub>0.49</sub>T. The enhancement of  $\sigma_b$  originates from oxygen vacancies generated according to the following Kroger–Vink equation



The  $\log_{10} \sigma_b - 1/T$  relationship of Sr-doped NB<sub>0.49</sub>T shows a change in activation energy at  $\sim 300$  °C, which is also observed in undoped and Mg-doped NB<sub>0.49</sub>T. This temperature is associated with a maximum in permittivity as observed from dielectric spectroscopy measurements;<sup>29</sup> however, the reason(s) for a change of activation energy around this temperature and the maximum in permittivity remain(s) unclear.

The crystallography, polymorphism, and polymorphic phase transition temperatures of NBT remain challenging topics. It is generally accepted that NBT undergoes a rhombohedral to tetragonal phase transformation at  $\sim 250$  °C; however, there is coexistence of the rhombohedral (R) and tetragonal (T) phases before it fully transforms into a single tetragonal phase at  $\sim 400$

°C, and finally undergoes a tetragonal to cubic (C) transition at  $\sim 520$  °C.<sup>34</sup> In the mixed phase region, generally considered to be  $\sim 250$  to 400 °C, the volume fraction of the T phase increases with increasing temperature, as revealed by neutron diffraction studies.<sup>35</sup>

R and T phase coexistence in this temperature range is confirmed by high-temperature electron diffraction studies on NB<sub>0.49</sub>T by TEM, Figure S5 through the observation of both strong  $1/2\{00e\}$  (tetragonal, *P4bm*) and  $1/2\{00o\}$  (rhombohedral, *R3c*) octahedral tilt superstructure reflections in which  $o = \text{odd}$  and  $e = \text{even}$ . Competition between T and R phases results in disorder of the octahedral tilting, resulting in additional streaking along the [100] direction.

Considering a two-phase composite with  $\sigma_{(R)}$  and  $\sigma_{(T)}$  representing the bulk conductivity of the two phases and using the volume fraction of each phase from a powder diffraction study in ref 35., an estimation of the total  $\sigma_b$  for NB<sub>0.49</sub>T and Sr-doped NB<sub>0.49</sub>T from the Maxwell model<sup>36</sup> gives reasonable agreement with the experimental data, Figure S6. Coexistence of R and T phases is a plausible explanation for the change in activation energy of  $\sigma_b$  at  $\sim 300$  °C and for the maximum in the permittivity data at  $\sim 325$  °C; however, further evidence, i.e., volume fractions of R and T phases in NB<sub>0.49</sub>T and Sr-doped NB<sub>0.49</sub>T from neutron diffraction and/or TEM, are required and are in progress.

Comparing with other oxide-ion conductors below 300 °C,  $\sigma_b$  of Sr-doped NB<sub>0.49</sub>T is  $\sim 2$  orders of magnitude higher than (BiO<sub>1.5</sub>)<sub>0.8</sub>(ErO<sub>1.5</sub>)<sub>0.2</sub>, 20ESB and  $\sim 1$  order of magnitude higher than (BiO<sub>1.5</sub>)<sub>0.88</sub>(DyO<sub>1.5</sub>)<sub>0.08</sub>(WO<sub>3</sub>)<sub>0.04</sub>, 8D4WSB, Figure 1. At higher temperature, i.e., 500 °C,  $\sigma_b$  of Sr-doped NB<sub>0.49</sub>T is initially lower than 20ESB and 8D4WSB, however, it shows no appreciable degradation of  $\sigma_b$  with time contrary to the rapid conductivity degradation of 20ESB and 8D4WSB, Figure 2a. It is noteworthy that undoped NB<sub>0.49</sub>T also shows negligible degradation of  $\sigma_b$  at 500 °C, albeit with a lower magnitude of conductivity due to its lower level of oxygen vacancies, Figure 2a. The conductivity degradation of stabilized  $\delta$ -Bi<sub>2</sub>O<sub>3</sub> at  $\sim 500$  °C is primarily attributed to the ordering of the oxygen sublattice<sup>26</sup> that can be alleviated by increasing dopant concentration,<sup>23,27,28</sup> for example, 25D5WSB shows the best stability and the highest long-term conductivity.<sup>28</sup> Considering the price and availability of rare-earth oxides such as Dy<sub>2</sub>O<sub>3</sub>, Sr-doped NB<sub>0.49</sub>T is competitive as a more sustainable material with only slightly lower conductivity than 25D5WSB, Figure 2a.

The degradation of  $\sigma_b$  for Sr-doped NB<sub>0.49</sub>T at various temperatures is shown in Figure 2b. In the temperature range studied (200–500 °C),  $\sigma_b$  shows no appreciable degradation with time apart from a slight depression of conductivity at 300 °C. The degradation can be described by an empirical equation<sup>18,26</sup>

$$\sigma(t) = \sigma(\infty) + [\sigma(0) - \sigma(\infty)]\exp[-(t/\tau)^\beta] \quad (2)$$

where  $t$  is time,  $\sigma(0)$  is the initial conductivity,  $\sigma(\infty)$  is the conductivity at infinite time,  $\beta$  is a dimensionless parameter, and  $\tau$  is the pertinent time constant. Fitting of  $\sigma_b - t$  data at 300 °C using Equation 2 gives a  $\sigma(\infty)/\sigma(0)$  of 0.79, Figure 2c, indicating  $\sim 80\%$  of  $\sigma_b$  is retained after long-term exposure at 300 °C. The conductivity decay at this temperature may be a consequence of the two-phase coexistence as discussed earlier and further work is ongoing to establish the origin of this low degradation at  $\sim 300$  °C. Nevertheless, NB<sub>0.49</sub>T-based perovskite oxide-ion conductors can achieve high oxide-ion conductivity at low levels of oxygen vacancy concentration,

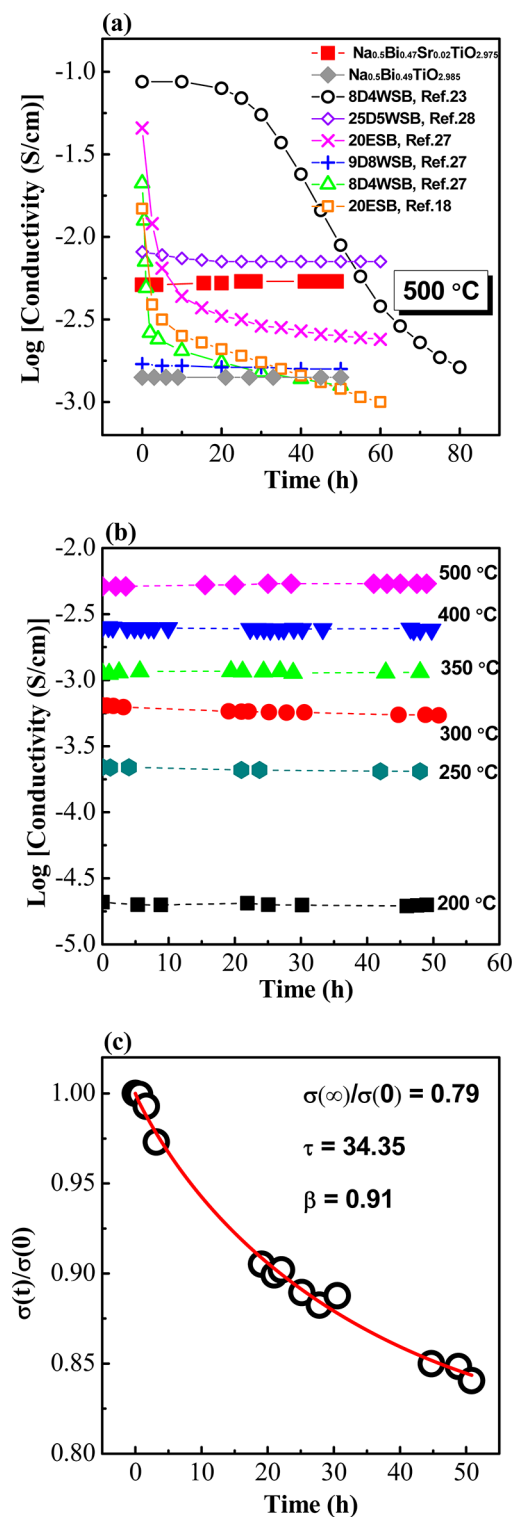


**Figure 2.** (a) Comparison of bulk conductivity stability at 500 °C for Sr-doped NB<sub>0.49</sub>T and selected Bi-based oxide-ion conductors: red square, Na<sub>0.50</sub>Bi<sub>0.47</sub>Sr<sub>0.02</sub>TiO<sub>2.975</sub> (Sr-doped NB<sub>0.49</sub>T), this work; grey diamond, Na<sub>0.50</sub>Bi<sub>0.49</sub>TiO<sub>2.985</sub> (NB<sub>0.49</sub>T), this work; open circle, 8D4WSB;<sup>23</sup> open diamond, 25D5WSB;<sup>28</sup> magenta ×, 20ESB;<sup>27</sup> blue cross, 9D8WSB;<sup>27</sup> green triangle, 8D4WSB;<sup>27</sup> orange open square, 20ESB.<sup>18</sup> (b) Bulk conductivity versus time of Sr-doped NB<sub>0.49</sub>T at selected temperatures. (c) Fitting curve and parameters of the conductivity decay for Sr-doped NB<sub>0.49</sub>T at 300 °C using eq 2. The open circles are experimental data and the red line is the fitting curve.

e.g., 0.5% in NB<sub>0.49</sub>T and 0.83% in Sr-doped NB<sub>0.49</sub>T compared to ~25% in  $\delta$ -Bi<sub>2</sub>O<sub>3</sub> fluorites. This dramatically suppresses the possibility of forming defect clusters or ordering of the anion sublattice, and therefore significantly improves the stability of the bulk conductivity in the important intermediate temperature range of ~400–600 °C for the development of ITSOFCs based on novel electrolytes.

Finally, the chemical stability of Sr-doped NB<sub>0.49</sub>T in reducing atmosphere, which is one of the major problems for Bi containing materials in developing ITSOFCs, has been investigated. XRD patterns of Sr-doped NB<sub>0.49</sub>T annealed in 5% H<sub>2</sub>/95%N<sub>2</sub> at various temperatures for 12 h are shown in Figure 3a. After annealing at  $\geq 600$  °C, an additional peak

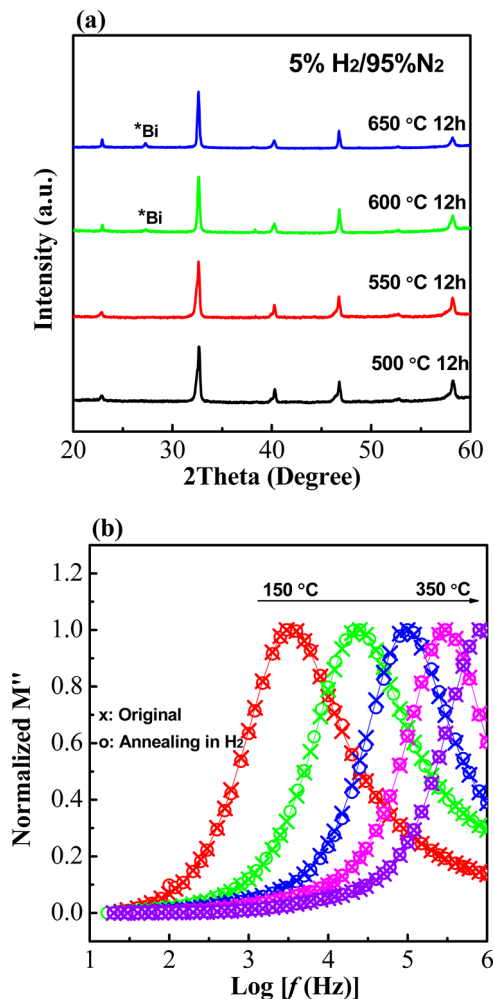


**Figure 3.** (a) XRD patterns of Sr-doped NB<sub>0.49</sub>T pellets after annealing in 5% H<sub>2</sub>/95% N<sub>2</sub> at various temperatures for 12 h; (b) M''-log f plots for Sr-doped NB<sub>0.49</sub>T before (cross) and after annealing (open circle) in 5% H<sub>2</sub>/95% N<sub>2</sub> at 550 °C for 12 h.

associated with Bi metal is detected, indicating that decomposition of the material has started to occur. In contrast, no additional reflection(s) were observed in XRD patterns for samples annealed at  $\leq 550$  °C. Furthermore, impedance measurements carried out on a pellet annealed at 550 °C in 5% H<sub>2</sub> for 12 h showed the bulk response in the M''-log f plots to be unchanged from those before annealing, Figure 3b. This supports the evidence from XRD that Sr-doped NB<sub>0.49</sub>T is chemically stable and can withstand 550 °C in 5% H<sub>2</sub>.

In conclusion, we report a Sr-doped  $\text{NB}_{0.49}\text{T}$  perovskite material that shows excellent ionic conductivity with extremely low levels of degradation and reasonable stability in a 5% $\text{H}_2$  reducing atmosphere at  $\leq 550$  °C. This demonstrates A-site acceptor doping to be as effective as B-site acceptor doping in enhancing the ionic conductivity of  $\text{NB}_{0.49}\text{T}$ . Although first-principles calculations predict A-site acceptor doping to be superior to B-site acceptor doping, results from this work do not support significant superiority of bulk conductivity by A-site acceptor doping. This might be due to the lower polarizability of  $\text{Sr}^{2+}$  ( $4.24 \text{ \AA}^3$ )<sup>37</sup> and higher Sr–O bond strength ( $454 \text{ kJ/mol}$ )<sup>38</sup> compared with that of  $\text{Bi}^{3+}$  ( $6.12 \text{ \AA}^3$ )<sup>37</sup> and Bi–O ( $343 \text{ kJ/mol}$ )<sup>38</sup>, which will also influence the mobility of the oxygen ions.

Compared with the two best known  $\delta\text{-Bi}_2\text{O}_3$  oxide-ion conductors, 8D4WSB and 20ESB, Sr-doped  $\text{NB}_{0.49}\text{T}$  perovskite shows competitive levels of oxide-ion conductivity at 500 °C with the advantage of insignificant degradation of the bulk conductivity at this temperature and it exhibits much higher bulk conductivity below 300 °C. Sr-doped  $\text{NB}_{0.49}\text{T}$  also has an advantage over these  $\delta\text{-Bi}_2\text{O}_3$  phases as a more sustainable (RE-free) material. Similar behavior is also observed for Ca and Ba-doped  $\text{NB}_{0.49}\text{T}$ . Further work is in progress to understand the relationship between phase-coexistence and conductivity between  $\sim 250$  and 400 °C, as well as to further enhance the conductivity of  $\text{NB}_{0.49}\text{T}$  via appropriate chemical doping.

## ■ ASSOCIATED CONTENT

### Supporting Information

The Supporting Information is available free of charge on the ACS Publications website at DOI: 10.1021/acs.chemmater.6b02555.

Details for sample preparation and experimental techniques; results of XRD, SEM, EDX, impedance spectroscopy measured at various atmospheres, ionic transport numbers, variable-temperature TEM, and fitting of  $\sigma_b$  using Maxwell model (PDF)

## ■ AUTHOR INFORMATION

### Corresponding Author

\*E-mail: d.c.sinclair@sheffield.ac.uk.

### Author Contributions

The manuscript was written through contributions of all authors./All authors have given approval to the final version of the manuscript.

### Funding

The research is funded by EPSRC EP/L027348/1.

### Notes

The authors declare no competing financial interest.

## ■ REFERENCES

- Boivin, J. C.; Mairesse, G. Recently material developments in fast oxide ion conductors. *Chem. Mater.* **1998**, *10*, 2870–2888.
- Hibino, T.; Hashimoto, A.; Inoue, T.; Tokuno, J.; Yoshida, S.; Sano, M. A low-operating-temperature solid oxide fuel cell in hydrocarbon-air mixtures. *Science* **2000**, *288*, 2031–2033.
- Skinner, S. J.; Kilner, J. A. Oxygen ion conductors. *Mater. Today* **2003**, *6*, 30–37.
- Steele, B. C. H. Oxygen ion conductors and their technological applications. *Mater. Sci. Eng., B* **1992**, *13*, 79–87.
- Maskell, W. C. Progress in the development of zirconia gas sensors. *Solid State Ionics* **2000**, *134*, 43–50.

(6) Pham, A. Q.; Glass, R. S. Oxygen pumping characteristics of yttria-stabilized-zirconia. *Electrochim. Acta* **1998**, *43*, 2699–2708.

(7) Yamamoto, O.; Arachi, Y.; Sakai, H.; Takeda, T.; Imanishi, N.; Mizutani, Y.; Kawai, M.; Nakamura, Y. Zirconia Based Oxide Ion Conductors for Solid Oxide Fuel Cells. *Ionics* **1998**, *4*, 403–408.

(8) Arachi, Y.; Sakai, H.; Yamamoto, O.; Takeda, Y.; Imanishi, N. Electrical conductivity of the  $\text{ZrO}_2\text{-Ln}_2\text{O}_3$  (Ln = lanthanides) system. *Solid State Ionics* **1999**, *121*, 133–139.

(9) Kilner, J. A. Fast oxygen transport in acceptor doped oxides. *Solid State Ionics* **2000**, *129*, 13–23.

(10) Omar, S.; Wachsmann, E. D.; Jones, J. L.; Nino, J. C. Crystal structure-ionic conductivity relationships in doped ceria systems. *J. Am. Ceram. Soc.* **2009**, *92*, 2674–2681.

(11) Ishihara, T.; Matsuda, H.; Azmi bin Bustam, M.; Takita, Y. Oxide ion conductivity in doped Ga based perovskite type oxide. *Solid State Ionics* **1996**, *86–88*, 197–201.

(12) Huang, K.; Feng, M.; Goodenough, J. B.; Milliken, C. Electrode performance test on single ceramic fuel cells using as electrolyte Sr- and Mg-doped  $\text{LaGaO}_3$ . *J. Electrochem. Soc.* **1997**, *144*, 3620–3624.

(13) Ishihara, T.; Honda, M.; Shibayama, T.; Minami, H.; Nishiguchi, H.; Takita, Y. Intermediate temperature solid oxide fuel cells using a new  $\text{LaGaO}_3$  based oxide ion conductor. *J. Electrochem. Soc.* **1998**, *145*, 3177–3183.

(14) Lacorre, P.; Goutenoire, F.; Bohnke, O.; Retoux, R.; Lalignant, Y. Designing fast oxide-ion conductors based on  $\text{La}_2\text{Mo}_2\text{O}_9$ . *Nature* **2000**, *404*, 856–858.

(15) Nakayama, S.; Aono, H.; Sadaoka, Y. Ionic conductivity of  $\text{Ln}_{10}(\text{SiO}_4)_6\text{O}_3$  (Ln = La, Nd, Sm, Gd and Dy). *Chem. Lett.* **1995**, *24*, 431–432.

(16) Verkerk, M. J.; Keizer, K.; Burggraaf, A. J. High oxygen ion conduction in sintered oxides of the  $\text{Bi}_2\text{O}_3\text{-Er}_2\text{O}_3$  system. *J. Appl. Electrochem.* **1980**, *10*, 81–90.

(17) Verkerk, M. J.; Burggraaf, A. J. High oxygen ion conduction in sintered oxides of the  $\text{Bi}_2\text{O}_3\text{-Dy}_2\text{O}_3$  system. *J. Electrochem. Soc.* **1981**, *128*, 75–82.

(18) Jiang, N.; Wachsmann, E. D. Structural Stability and Conductivity of phase-stabilized cubic bismuth oxides. *J. Am. Ceram. Soc.* **1999**, *82*, 3057–3064.

(19) Jiang, N.; Wachsmann, E. D.; Jung, S. A higher conductivity  $\text{Bi}_2\text{O}_3$ -based electrolyte. *Solid State Ionics* **2002**, *150*, 347–353.

(20) Jung, D. W.; Duncan, K. L.; Wachsmann, E. D. Effect of total dopant concentration and dopant ratio on conductivity of  $(\text{DyO}_{1.5})_x\text{-(WO}_3)_y\text{-(BiO}_{1.5})_{1-x-y}$ . *Acta Mater.* **2010**, *58*, 355–363.

(21) Abraham, F.; Boivin, J. C.; Mairesse, G.; Nowogrocki, G. The BIMEVOX series: a new family of high performance oxide ion conductors. *Solid State Ionics* **1990**, *40-41*, 934–937.

(22) Wachsmann, E. D.; Ball, G. R.; Jiang, N.; Stevenson, D. A. Structural and defect studies in solid oxide electrolytes. *Solid State Ionics* **1992**, *52*, 213–218.

(23) Jung, D. W.; Duncan, K. L.; Camaratta, M. A.; Lee, K. T.; Nino, J. C.; Wachsmann, E. D. Effect of annealing temperature and dopant concentration on the conductivity behaviour in  $(\text{DyO}_{1.5})_x\text{-(WO}_3)_y\text{-(BiO}_{1.5})_{1-x-y}$ . *J. Am. Ceram. Soc.* **2010**, *93*, 1384–1391.

(24) Wachsmann, E. D.; Jayaweera, P.; Jiang, N.; Lowe, D. M.; Pound, B. G. Stable high conductivity ceria/bismuth oxide bilayered electrolytes. *J. Electrochem. Soc.* **1997**, *144*, 233–236.

(25) Wachsmann, E. D.; Lee, K. T. Lowering the temperature of solid oxide fuel cells. *Science* **2011**, *334*, 935–939.

(26) Wachsmann, E. D.; Boyapati, S.; Jiang, N. Effect of dopant polarizability on oxygen sublattice order in phase-stabilized cubic bismuth oxides. *Ionics* **2001**, *7*, 1–6.

(27) Jung, S. H.; Wachsmann, E. D.; Jiang, N. Structural stability and conductivity of cubic  $(\text{DyO}_{1.5})_x\text{-(WO}_3)_y\text{-(BiO}_{1.5})_{1-x-y}$ . *Ionics* **2002**, *8*, 210–214.

(28) Jung, D. W.; Nino, J. C.; Duncan, K. L.; Bishop, S. R.; Wachsmann, E. D. Enhanced long-term stability of bismuth oxide-based electrolytes for operation at 500 °C. *Ionics* **2010**, *16*, 97–103.

(29) Li, M.; Pietrowski, M. J.; De Souza, R. A.; Zhang, H.; Reaney, I. M.; Cook, S. N.; Kilner, J. A.; Sinclair, D. C. A family of oxide ion

conductors based on the ferroelectric perovskite  $\text{Na}_{0.5}\text{Bi}_{0.5}\text{TiO}_3$ . *Nat. Mater.* **2014**, *13*, 31–35.

(30) Li, M.; Zhang, H.; Cook, S. N.; Li, L.; Kilner, J. A.; Reaney, I. M.; Sinclair, D. C. Dramatic influence of A-site Nonstoichiometry on the electrical conductivity and conduction mechanisms in the perovskite oxide  $\text{Na}_{0.5}\text{Bi}_{0.5}\text{TiO}_3$ . *Chem. Mater.* **2015**, *27*, 629–634.

(31) Dawson, J. A.; Chen, H.; Tanaka, I. Crystal structure, defect chemistry and oxygen ion transport of the ferroelectric perovskite,  $\text{Na}_{0.5}\text{Bi}_{0.5}\text{TiO}_3$ : insights from first-principles calculations. *J. Mater. Chem. A* **2015**, *3*, 16574–16582.

(32) He, X.; Mo, Y. Accelerate materials design of  $\text{Na}_{0.5}\text{Bi}_{0.5}\text{TiO}_3$  oxygen ionic conductors based on first principles calculations. *Phys. Chem. Chem. Phys.* **2015**, *17*, 18035–18044.

(33) Zhang, T.; Hing, P.; Huang, H.; Kilner, J. A. Ionic conductivity in the  $\text{CeO}_2$ - $\text{Gd}_2\text{O}_3$  system ( $0.05 \leq \text{Gd}/\text{Ce} \leq 0.4$ ) prepared by oxalate coprecipitation. *Solid State Ionics* **2002**, *148*, 567–573.

(34) Suchanicz, J.; Kwapulinski, J. X-ray diffraction study of the phase transitions in  $\text{Na}_{0.5}\text{Bi}_{0.5}\text{TiO}_3$ . *Ferroelectrics* **1995**, *165*, 249–253.

(35) Jones, G. O.; Thomas, P. A. Investigation of the structure and phase transitions in the novel A-site substituted distorted perovskite compound  $\text{Na}_{0.5}\text{Bi}_{0.5}\text{TiO}_3$ . *Acta Crystallogr., Sect. B: Struct. Sci.* **2002**, *58*, 168–178.

(36) Maxwell, J. C. *A Treatise on Electricity and Magnetism*; Clarendon Press: Oxford, U.K., 1881.

(37) Grimes, N. M.; Grimes, R. W. Dielectric polarizability of ions and the corresponding effective number of electrons. *J. Phys.: Condens. Matter* **1998**, *10*, 3029–3034.

(38) Luo, Y. R. *Comprehensive Handbook of Chemical Bond Energies*; CRC Press: Boca Raton, FL, 2007.